

Reconstruction of potential from dynamic experiments

V. L. Popov,¹ J. Starcevic,¹ and A. E. Filippov²

¹*Technische Universität Berlin, Strasse des 17. Juni 135, D-10623 Berlin, Germany*

²*Donetsk Institute for Physics and Engineering NASU, 83114, Donetsk, Ukraine*

(Received 19 February 2007; revised manuscript received 15 April 2007; published 14 June 2007)

In experimental studies of a surface by an underdamped mechanical surface force probe the “tip” can return repeatedly to the same points in space. This causes a problem in using the experimental data to extract information about the surface structure. We propose an approach which allows one to extract the mesoscopic surface structure from dynamic experiments with underdamped systems. The approach was tested on numerically generated random fractal potentials and is applied to extract potential relief from real experimental data.

DOI: [10.1103/PhysRevE.75.066104](https://doi.org/10.1103/PhysRevE.75.066104)

PACS number(s): 81.40.Pq, 68.35.Bs, 46.55.+d, 68.35.Af

INTRODUCTION

In this work we study the problem of how to use experimentally measured time sequences of force to reconstruct the physical potential responsible for this force. Specifically, the problem is studied here in underdamped systems. Such a problem can appear in systems where an inertial contribution to the measured force is non-negligible. This contribution has a strong quasirandom impact on the time sequence and drastically masks the potential force to be reconstructed. This study focuses on the extraction of surface structure information from tribological experiments, a fundamental theoretical problem in the dynamics of systems with a complex random (fractal) structure. It has important practical applications, e.g., in micromechanical and ultrasonic devices [1]. As a mathematical tool we use the simple Tomlinson model, widely used as a model of friction [2].

In spite of its simplicity, the Tomlinson model describes many essential features of tribological systems and has been utilized by many authors [1,3–15]. Recently developed experimental tools allow for the investigation of friction at nanometer scale and have stimulated many advances in understanding the relationship between macroscopic frictional forces and microscopic properties of systems [1,8,9,13–16]. The Tomlinson equation ordinarily operates with linear velocity dependence of microscopic dissipative forces. Physically, these forces are stemming from electron or phonon scattering processes and exist mainly on the microscopic level. The Langevin-type Tomlinson equation has thus been proven to provide a good basis in describing tribological experiments using a surface force apparatus, which moves and interacts on the atomic potential scale [10–12]. It is conversely not enough when we try to extend the study into mesoscopic scale. This situation appears often in practical mechanical tribological experiments. The model in its original form describes one degree of freedom and assumes a single contact point. In reality, many asperities are pulled over many other asperities, rendering the reconstruction of microscopic potential from such experiments impossible. The procedure may, however, be applied to reconstruct a coarse-grained surface structure at mesoscopic scale.

The model should be modified for mesoscopic scales by a specific renormalization of the velocity dependent friction and the addition of an effective dry (Coulomb) friction term

[21]. When the experimental scale is sufficiently far from atomic, friction becomes almost independent of sliding velocity. In a first approximation it is therefore plausible to represent friction using only a dry friction force. Nevertheless, in a typical scenario the surface force probe (or “tip”) returns repeatedly to the same space points. This important problem is related to the underdamped nature of the motion, characteristic of a mesoscopic scale combined with dry friction. This fact causes additional difficulty in using the experimental data to extract surface structure information.

In this paper we propose a practical numerical procedure which allows the reconstruction of surface structure from the experiment and acquisition of the effective equation’s phenomenological friction parameter in a self-consistent manner. As an illustration, the approach is applied to an analysis of real experimental data. The test application results in a fractal structure of the reconstructed potential.

MODEL AND EQUATIONS

Let us start from a generalized equation of motion from the Tomlinson model in the following form:

$$\partial^2 x / \partial t^2 + (\eta + \gamma_{eff} |\partial x / \partial t|) \text{sgn}(\partial x / \partial t) + \partial U(x) / \partial x + K(x - Vt) = 0. \quad (1)$$

Here a driven plate of mass $M=1$ and the center-of-mass coordinate X is pulled by a spring with spring constant K . $U(X)$ is the effective potential experienced by the plate due to the presence of an embedded system. The spring is connected to a platform which moves at velocity V . The parameter γ_{eff} is responsible for a “standard” velocity dependent dissipation and η is the Coulomb friction constant.

An important feature of a realistic system is that the mesoscopic structure of frictional surfaces has fractal character [17,18]. The structure thereby cannot be characterized by one definite wave vector (or even a few wave vectors [1,3,8,9]) as normally presumed in applications of the Tomlinson model. The model must be extended to incorporate a realistic fractal potential. In numerical simulation it can be generated in the form [17]

$$U(x) = U_{fractal} = U_0 \int_{q_1}^{q_2} dq c(q) \cos(qx + \zeta), \quad c(q) = q^{-\beta}. \quad (2)$$

Here q_1 and q_2 are characteristic cutoff wave vectors and $\zeta(x)$ is a random phase that we assume to be δ -correlated $\langle \zeta(q)\zeta(q') \rangle = 2\pi\delta(q-q')$.

Below, this modified model is applied to simulate friction on a mesoscopically rough surface. This is certainly a three- or at least two-dimensional problem, but the main ideas can be shown well by a one-dimensional system. We have recently shown the model can be adapted to intermediate scales by the renormalization of velocity dependent friction and the addition of an effective dry friction force [21]. The effective potential in this case corresponds to a smoothed initial potential (obtained by means of exclusion of an appropriate number of Fourier modes). It is proven that in studying mesoscopic friction, one may represent a system using only dry friction ($\gamma \rightarrow 0$) [21]. In principle if to analyze mesoscopic experiments only, one can concentrate on this limit. It is relatively simple and all the numerical procedure in this case is more transparent. However, below we will return to the form $(\eta + \gamma|\partial x/\partial t|)\text{sgn}(\partial x/\partial t)$ of general interest also.

In an actual numerical study, the integral in Eq. (2) transforms into a sum: $\int dq c(q) \rightarrow \sum q$. Here a discrete step between the wave vectors Δq is determined by the smallest vector q_1 . This corresponds to an inverse maximum system length l_{max} which equates normally to its size $l_{max} = L$. The total number N_{tot} of the terms in the sum is given by $N_{tot} = q_2/q_1 \equiv q_2/\Delta q$.

The discrete technique is also logical for an analysis of experimental data. The data are automatically presented in the form of limited discrete arrays. This allows us to adjust the potential according to the actual size of the system, to a period of time N_t , and N_x number of space steps available in the data set. Further, for the general theoretical approach it is also important to be able to extend a procedure as necessary to as long time-space runs. That is, numerically generated fractal potential $U_{fractal}(x)$ should be extendable to an infinite run. For this sake, instead of Eq. (2), one may use the following differential definition of fractal potential: $\partial U_{fractal}(x)/\partial x = U_0 \Delta x \sum_j q_j c(q_j) \sin(q_j x + \xi)$, where $j=1, 2, \dots, N_{modes}$. This procedure naturally extends $U_{fractal}(x)$ a potentially infinite number of times, each time the x coordinate runs out of the array bonds. For numerical procedure it means that the modified Tomlinson equation

$$\partial^2 x/\partial t^2 + \eta \text{sgn}(\partial x/\partial t) + \partial U_{fractal}(x)/\partial x + K(x - Vt) = 0 \quad (3)$$

is actually accompanied by an additional differential equation which is solved in parallel.

RESULTS AND DISCUSSION

If the potential is fixed and external force ‘‘turns on’’ at some moment in time, Eq. (3) completely defines the motion. There is then a correlation between the experimentally recorded motion scenario and surface potential. However, we are interested in a solution of the inverse problem which restores the potential from the dynamic scenario. The inverse solution is not as straightforward as the direct solution. The main difficulty stems from the inertia of the system. This is

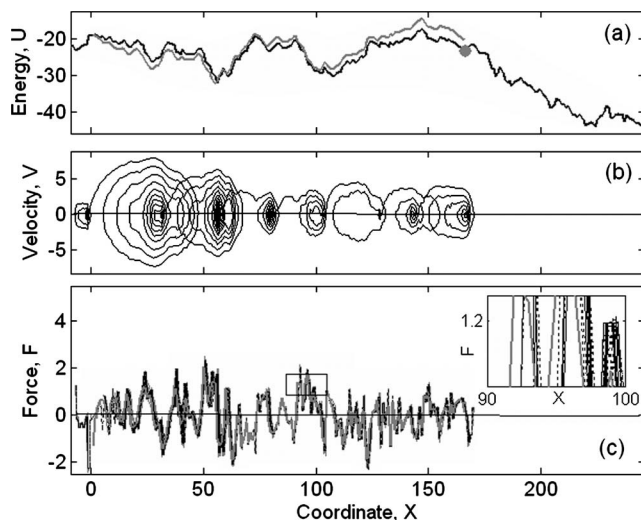


FIG. 1. Random potential (a), trajectory of motion in phase space $\{X, V\}$ (b), and projection of the force $F_{potential}[X(t_j)]$ to the $\{F, X\}$ plane (c), shown in dimensionless units. The gray line in subplot (a) depicts the potential according to a procedure described in the text. The black solid and dotted lines in the subplot (c) show numerically generated correct curve $F_{potential}[X]$ and the curve $F_{potential}[X(t_j)]$ found from the course-grained data. The bold gray curve in the same plot corresponds to the averaged potential force $F_{potential}(X) = \langle F_{potential}[X(t_j)] \rangle$.

evident in Figs. 1(a)–1(c). The numerically generated random potential is shown together with the trajectory of motion in phase space $\{X, V\}$ [Fig. 1(b)] and a projection of the potential component of force $F_{potential}[X(t_j)]$ on the X coordinate. Dimensionless units normalized to characteristic microscopic scales and energies of a particular system are used in these plots for general theoretical study.

Phase portrait technique, applied in Fig. 1(b), is often used in the closely related studies of dynamics in periodic or nonperiodic potentials (i.e., studies of the Frenkel-Kontorova model [19,20]). It allows one to record and observe clearly the whole dynamic history of very complex systems. In this particular case we can read from the plot how external force $F_{ext} = K(x - Vt)$ pulls a probe from one local minimum of the potential to another. The probe leaves its current minimum when the force exceeds a barrier and then flies to some other minimum determined by the next local equilibrium. After overcoming the barrier it falls down with a nonzero velocity which it maintains for a while due to inertia.

Again, if the scale is sufficiently far from atomic, the friction becomes nearly independent of the sliding velocity and can be approximated by a dry friction force. As a result, the scenario is defined by a complex combination of the external force F_{ext} , potential relief $U(x)$, and friction force $F_{friction} = \eta \text{sgn}(\partial x/\partial t)$. Despite neglecting the velocity dependent part of the dissipation γ_{eff} in Eq. (3), the energy of this externally driven system does not grow with time. The behavior of the system is stabilized due to the friction force $F_{friction} = \eta \text{sgn}(\partial x/\partial t)$, which provides a dissipative force at every moment of the process.

Nonlinearity of the potential and changeable balance of all the forces produces extremely complex dynamic behav-

ior. It is difficult to predict both the position of the next local equilibrium and the number of oscillations before the next stop. The flow line repeatedly visits the same positions of the space X with different velocity at every visit.

Despite the complexity of this motion, one may formally accumulate numerical (or experimental) arrays of the coordinate $X(t_j)$ and force $F_{ext}(t_j)$ and combine them according to a discrete analog of Eq. (3) as follows:

$$F_{potential} = F_{potential}[X(t_j)] = (X_{j+1} + X_{j-1} - 2X_j)/dt_j^2 + \eta \operatorname{sgn}(V_j) + K(X_j - Vt_j), \quad (4)$$

where $dt_j = t_{j+1} - t_j$; $V_j = (X_{j+1} - X_j)/dt_j$. Formally applied, the numerical procedure is to completely define the function $F_{potential} \equiv \partial U_{fractal}(X)/\partial X$. One can plot the array $F_{potential}$ as a parametric function of the coordinate $F_{potential} = F_{potential}[X(t_j)]$, as done in Fig. 1(c). The plot gives a visual representation of the actual spatial dependence of $F_{potential}$ and provides a basis for further operations.

Due to a loss of information caused by discrete implementation, the force $F_{potential}$ always has a few close, but still different values at every coordinate point. Black solid and dotted lines in Fig. 1(c) show the true (original) numerically generated curve $F_{potential}[X]$ and the curve of less refined $F_{potential}[X(t_j)]$ for a comparison. A magnified portion of the data shown in a rectangle within Fig. 1(c) makes the fine structure of the force more readily visible.

The procedure mainly involves calculating the number of values in every segment of the coordinate array $\{X(I)\}$, accumulating the total sum of the force impacts from all the visits of the same segment, and normalizing this sum according to the number of visits. Applying this procedure to the whole array yields an averaged potential force $F_{potential}(X) = \langle F_{potential}[X(t_j)] \rangle$. The bold gray curve in Fig. 1(c) corresponds to the result obtained. Now we can use this mean force $F_{potential}(X)$ to find the effective potential by integration as follows:

$$U_{eff}(X) = \int_{X_0}^X dX F_{potential}(X). \quad (5)$$

The gray line in Fig. 1(a) depicts the reconstructed potential structure to compare it with the generated structure, represented by the black line. To simulate naturally limited information of an experimental array, this potential is restored using $N_t^{reduced}/N_t = 10^{-2}$ points of the numerically produced dependencies calculated according to dynamic Eq. (3). This results in a loss of information, causing reconstructed potential to deviate from the exact initial potential. It is worthy to note, though, that even for the very significant reduction of information $N_t^{reduced}/N_t = 10^{-2}$ the result still reproduces the correct potential quite well. This is important in the context of further applications, where we are always limited by experimental data and do not know the correct potential *a priori* to compare with.

The reduction of information is important also in a context of thermal noise which exists in any real system. The noise term is not written in Eq. (1) of the article, but we checked its role in numerical simulations. To some extent it

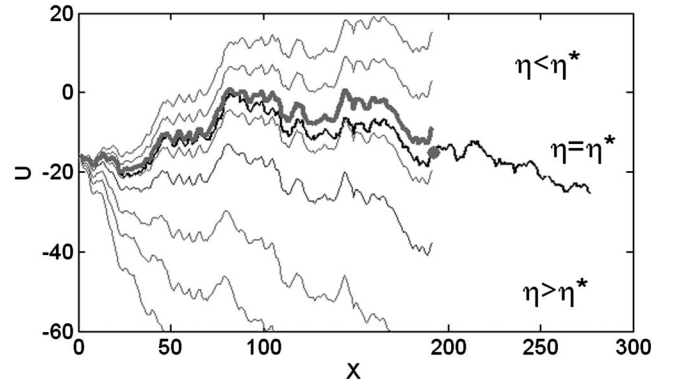


FIG. 2. A family of potentials restored from the procedure at different trial η values. Numerically generated correct potential is shown by the black line. Restored potential corresponding to the known exact η^* value is represented by the bold gray line.

plays here the same role as a dynamic chaos in the system under consideration and opens just an additional channel for the chaotic impacts. When temperature noise is relatively weak it causes fluctuations of the scanning probe inside of every potential minimum only. The procedure, which is based on a coarse grained description, averages additional random impacts to the velocities as well, and the result almost does not depend on the noise. As is expected, we found a threshold effect of the temperature. When random impact to kinetic energy exceeds a potential barrier the probe can uncontrollably jump from one minimum to another and restored potential starts to diverge from a correct one.

Also noteworthy is that the discrete analog of the dynamic Eq. (4) and said procedure involve previous knowledge of a correct parameter η . In the case of a real experiment this value is not known in advance. However, as we show below, it can be found within the course of the same procedure that restores the potential.

The equation of motion and phase portrait in Fig. 1(b) show directly that if the constant η is chosen incorrectly, but the time data sequence corresponds to a real physical scenario, the friction component $F_{friction} = \eta \operatorname{sgn}(\partial x / \partial t)$ of the total force will systematically either overestimate or underestimate kinetic impact on the total potential. As result, the potential $U_{eff}(X) = \int_{X_0}^X dX F_{potential}(X)$, integrated using reconstructed force, will systematically increase (or decrease) along the coordinate X .

To observe this discrepancy, we have performed such a calculation for a numerically generated potential and an array of different parameters η . It produces a family of the potentials corresponding to different η values, presented in Fig. 2. The numerically generated correct potential is shown here by a black line. Only one η corresponds to the correct η^* value (known here in advance) and only one potential lies close to the correct one. This potential is shown by the bold gray line in the figure. All other curves stray either up or down along the space coordinate X , as expected.

This observation gives a receipt which allows one to restore both the microscopic friction force and the correct surface potential from the same tribological experiment. It is applied to the processing of real friction data obtained from

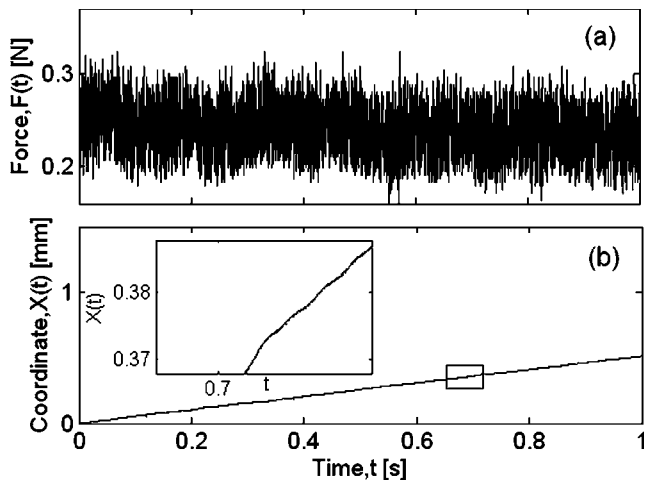


FIG. 3. Experimental data of (measurable) external force $F_{ext} = K(x - Vt)$ (a) and coordinate $X(t_j)$ (b) used to apply the proposed procedure. Coordinates are measured in millimeters, time in seconds, and force in newtons. A magnified view to the curve $X(t_j)$ is shown in the rectangular inset to subplot (b). A corresponding piece of the main plot is enclosed by a second rectangle.

experiments described below. We used the experimental setup set forth in [17]. A steel sample was dragged along a steel plate with a spring, the coordinate of the sample was measured with a laser vibrometer at a frequency of 10^5 measurements per second, and the spring force was measured with a force sensor. The results are summarized in Figs. 3–5. Experimental data of (measurable) external force $F_{ext} = K(x - Vt)$ and coordinate $X(t_j)$ being used to apply the above procedure are presented in Fig. 3(a) and 3(b), respectively. The coordinate in the plot is measured in millimeters, time in seconds, and force in newtons. The coordinate $X(t_j)$ grows linearly with time, making its fine structure essentially indis-

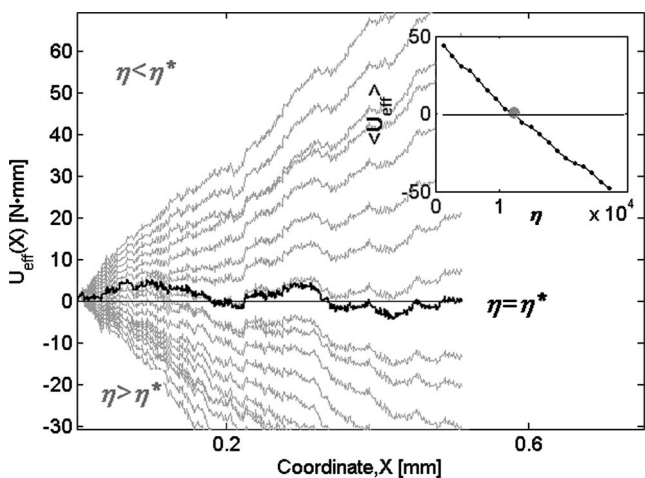


FIG. 4. A family of potentials $U_{eff}(X)$ restored using experimental data at different trial η values. The mean value of the potentials $\langle U_{eff}(X) \rangle$ is plotted versus η in the inset. The expected correct value of $\eta = \eta^*$ corresponding to the $\langle U_{eff}(X) \rangle$ closest to zero, $\langle U_{eff}(X) \rangle \approx 0$, is marked by the gray circle. The potential $U_{eff}(X)$ corresponding to this value is shown by the black line in the main plot.

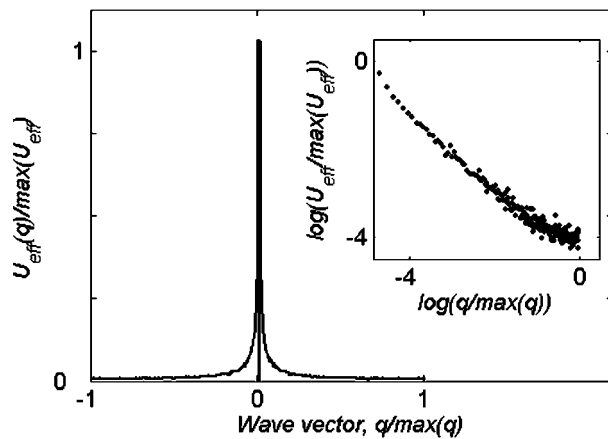


FIG. 5. Fourier transform of the potential $U_{eff}(q)$ and its log-log plot, shown in the rectangular inset, which illustrates that $U_{eff}(q)$ has a fractal spectral density $C(q) \propto q^\beta$.

tinguishable in Fig. 3(b). To make it clearer, we again include a magnified portion inside a rectangle within Fig. 3(b).

A family of the potentials $U_{eff}(X)$ restored using the experimental data for different trial η values is shown in Fig. 4. The correct result must follow a real physical potential, which should be approximately horizontal. In other words, it does not systematically grow or decrease and its mean value is closer to zero than mean potentials corresponding to other incorrectly chosen η values.

We have calculated the mean values of the potentials $\langle U_{eff}(X) \rangle$ at different constants η and plotted them in the rectangular inset to Fig. 4. The value of $\eta \approx \eta^*$ has been estimated from the condition $\langle U_{eff}(X) \rangle \approx 0$. This value is marked by the gray circle in the inset. The resulting potential $U_{eff}(X)$ corresponding to the value $\eta \approx \eta^*$ is shown by the black line in the main plot.

It is well known that the majority of the physical surfaces have universal fractal structure, [17,18] and physical potential is expected to have a fractal spectral density $C(q) \propto q^\beta$. It is interesting to analyze from this point of view the potential obtained. To do this, we have calculated the Fourier transform of the potential $U_{eff}(X) \rightarrow U_{eff}(q)$. The result is presented in Fig. 5. It has almost perfect power-law shape which can be checked additionally using a log-log plot, shown in the rectangular inset. The distribution of points in the inset deviates from the straight line at high and low wave vectors q . This is quite natural for the restricted set of the experimental data, which is used to restore the potential, and limited on both sides by the length of the recorded run and minimum space-time resolution. The same procedure has been repeated for a number of experimental data sequences. In all cases, qualitatively, it gives the same results. An effective exponent β recovered from the logarithmic plots lies in the interval $0.75 \leq \beta \leq 1.0$, which is in agreement with the results found in other approaches.

Our experiments were performed on a mesoscopic level. We therefore assumed that the dominant frictional force is velocity independent dry friction $\eta \operatorname{sgn}(\partial x / \partial t)$, and the only unknown parameter to be found is η . In general case (especially in nanoscale systems) the friction force can have a

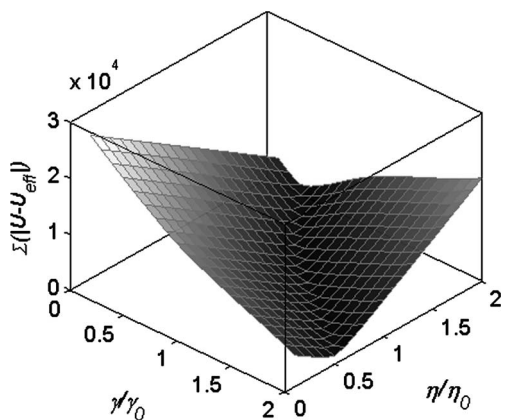


FIG. 6. Total deviation of the potential $U_{eff}(X; \eta, \gamma)$ from trial one accumulated along an interval of motion $\{X\}$: $D(\eta, \gamma) = \sum_X |U(X) - U_{eff}(X; \eta, \gamma)|$ as a function of the parameters η and γ .

velocity dependent contribution of the form $\gamma |\partial x / \partial t| \text{sgn}(\partial x / \partial t)$. It is important to generalize the above algorithm to include both contributions to friction. To this end we repeated all the procedure varying both parameters η and γ [for the same numerically generated dynamic set $x(t)$]. If we fix one of the parameters (let us say $\eta = \text{const}$) and vary γ , we obtain qualitatively the same families of the potential such as shown in Fig. 2. The results of these calculations are summarized in Fig. 6. It presents the total deviation of the potential $U_{eff}(X; \eta, \gamma)$ from the trial one accumulated along the interval of motion $\{X\}$ as follows:

$$D(\eta, \gamma) = \sum_X |U(X) - U_{eff}(X; \eta, \gamma)|$$

as a function of the parameters η and γ . For an arbitrary pair of the parameters, the restored potential $U_{eff}(X; \eta, \gamma)$ grows or decreases with the coordinate X . Numerical simulation shows that there is a line $\gamma = \gamma(\eta)$ at the parameters plane (η, γ) along which $U_{eff}(X; \eta, \gamma)$ matches $U(X)$ almost perfectly.

It means that both contributions to the friction similarly affect the reconstructed effective potential. If one of the parameters is wrong and systematically either overestimate or

underestimate kinetic impact on the total potential $U_{eff}(X; \eta, \gamma)$ another one can be chosen to compensate its deviation from the correct one. In other words, we can restore the correct potential without knowing the detailed friction law, in formally the same procedure as before. We fix some value of one of the parameters η or γ and adjust a second one to get almost horizontal resulting potential. This procedure does not provide correct damping constants, but it restores the correct potential.

Let us discuss briefly the influence of thermal noise on the quality of potential reconstruction. Thermal noise can be described by an additional stochastic term in Eq. (1). To some extent it plays the same role as dynamic chaos in the system under consideration or roughening the data due to accuracy of measurement. As the reconstruction procedure is robust to these factors, we expect that it will not be too sensitive to thermal noise. We have made additional simulations with thermal noise which gave the following results. (a) When thermal noise is relatively weak it causes fluctuations of the scanning probe inside of every potential minimum only. The procedure which is based on a coarse grained description averages additional random impacts to the velocities as well, and the result almost does not depend on the noise. (b) When random impact to kinetic energy exceeds a potential barrier, the probe begins to jump from one minimum to another and restored potential starts to diverge from a correct one.

In summary, we have proposed a method which allows the reconstruction of surface structure from dynamic experiments in the case of underdamped systems where the probe repeatedly returns to the same coordinate positions. The approach is studied in detail on numerically generated random fractal potentials where all the results and approximations are under complete control. It is applied further to real experimental data for which a physical potential relief is extracted with satisfactory accuracy.

ACKNOWLEDGMENTS

One of the authors (A.F.) is grateful to the Deutsche Forschungsgemeinschaft and European Science Foundation for financial support during his stay at Berlin Technological University.

-
- [1] B. N. J. Persson, *Sliding Friction, Physical Properties and Applications* (Springer, Berlin, 2000).
 - [2] G. A. Tomlinson, *Philos. Mag.* **7**, 905 (1929).
 - [3] M. G. Rozman, M. Urbakh, and J. Klafter, *Phys. Rev. Lett.* **77**, 683 (1996).
 - [4] V. Zaloj, M. Urbakh, and J. Klafter, *Phys. Rev. Lett.* **81**, 1227 (1998).
 - [5] M. Weiss and F. J. Elmer, *Phys. Rev. B* **53**, 7539 (1996).
 - [6] V. Zaloj, M. Urbakh, and J. Klafter, *Phys. Rev. Lett.* **82**, 4823 (1999).
 - [7] H. G. E. Hentschel, F. Family, and Y. Braiman, *Phys. Rev. Lett.* **83**, 104 (1999).
 - [8] M. Porto, M. Urbakh and J. Klafter, *Europhys. Lett.* **50**, 326 (2000).
 - [9] E. Gnecco R. Bennewitz, T. Gyalog, C. Loppacher, M. Bamberlin, E. Meyer, and H. J. Guntherodt, *Phys. Rev. Lett.* **84**, 1172 (2000).
 - [10] A. E. Filippov, J. Klafter, and M. Urbakh, *Phys. Rev. Lett.* **92**, 135503 (2004).
 - [11] A. E. Filippov, J. Klafter, and M. Urbakh, *Phys. Rev. Lett.* **87**, 275506 (2001).
 - [12] Z. Tshiprut, A. E. Filippov, and M. Urbakh, *Phys. Rev. Lett.* **95**, 016101 (2005).
 - [13] M. H. Muser, L. Wenning, and M. O. Robbins, *Phys. Rev. Lett.*

- 86**, 1295 (2001).
- [14] M. H. Muser, Phys. Rev. Lett. **89**, 224301 (2002).
- [15] C. Daly, J. Zhang, and J. B. Sokoloff, Phys. Rev. Lett. **90**, 246101 (2003).
- [16] A. Socoliuc, R. Bennewitz, E. Gnecco, and E. Meyer, Phys. Rev. Lett. **92**, 134301 (2004).
- [17] V. L. Popov and Ya. Starcevic, Tech. Phys. Lett. **31**, 309 (2005).
- [18] O. K. Dudko, V. L. Popov, and G. Putzar, Tribol. Int. **39**, 456 (2006).
- [19] H. Risken, *The Fokker-Planck Equation* (Springer, Berlin, 1996).
- [20] O. M. Braun and A. G. Naumovets, Surf. Sci. Rep. **60**, 79 (2006).
- [21] A. E. Filippov and V. L. Popov, Phys. Rev. E **75**, 027103 (2007).